LETTER

Unveiling the Impacts of Charge/Discharge Rate on the Cycling Performance of Li-Metal Batteries

Yunya Zhang,[#] Wurigumula Bao,[#] Ethan Jeffs, Bin Liu, Bing Han, Weijie Mai, Xinyu Li, Weikang Li, Yun Xu, Bhargav Bhamwala, Alex Liu, Louis Ah, Kun Ryu, Ying Shirley Meng,* and Hong Gan*
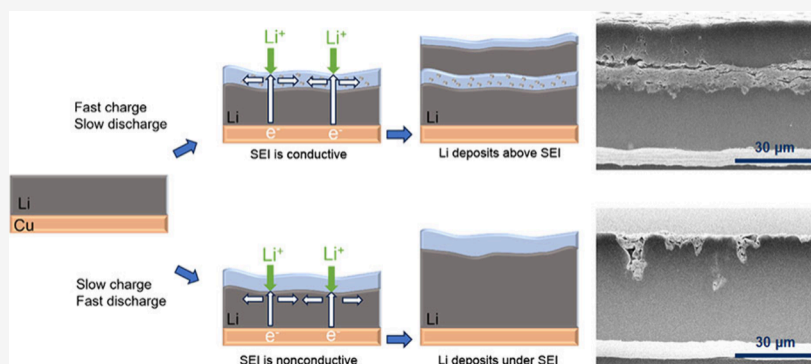
Read Online

ACCESS | Metrics & More | Article Recommendations | SI Supporting Information

ABSTRACT: Lithium metal batteries (LMBs) offer superior energy density and power capability but face challenges in cycle stability and safety. This study introduces a strategic approach to improving LMB cycle stability by optimizing charge/discharge rates. Our results show that slow charging (0.2C) and fast discharging (3C) significantly improve performance, with a multilayer LMB retaining over 80% capacity after 1000 cycles. Fast discharge rates promote lithium plating beneath the SEI layer, suppressing its growth and improving Coulombic efficiency, whereas slow discharge rates facilitate lithium plating above the SEI, leading to SEI accumulation. We propose a rational hypothesis linking SEI conductivity and cycling conditions and introduce an intermittent pulse discharge protocol to emulate electric vehicle applications, further improving the stability. These optimized cycling strategies enhance the LMB lifespan, utility, and safety, paving the way for broader market adoption in the years ahead.

Replacing the negative graphite electrode with lithium (Li) metal, which has 10 times higher capacity (374 mAh·g^{-1} vs 3860 mAh·g^{-1}), has been considered for decades as the ultimate solution for high energy batteries and therefore applicable for many electronic applications, especially long-range EVs.[1−3] However, the progress is in fact slow and unsatisfactory since there are still no commercial LMBs in the market.[3−5] One of the primary challenges in Li metal batteries is the formation of an unstable solid—electrolyte interphase (SEI). This passive layer forms when the Li metal surface comes into contact with the electrolyte, which is designed to prevent further reactions at the interface. Ideally, the SEI should be dynamically stable, conducting only ions while isolating electrons.[6,7] However, significant volume changes associated with uneven Li plating and stripping disrupt this dynamic balance. This disruption requires compensatory

reactions that gradually consume the Li and electrolyte inventory within the battery cycle-by-cycle, leading to a lower Coulombic efficiency (CE) of LMBs compared to those using graphite electrodes, such as Li-ion batteries.[6] The low Li cycling CE, which is often reported to be around 98−99.5%,[7] results in the unsatisfactory cycling life of LMBs. With a thin Li reservoir and a lean electrolyte, LMBs often achieve only about 100 cycles. Furthermore, the SEI residue tends to accumulate upon cycling, forming a thick, porous "inactive
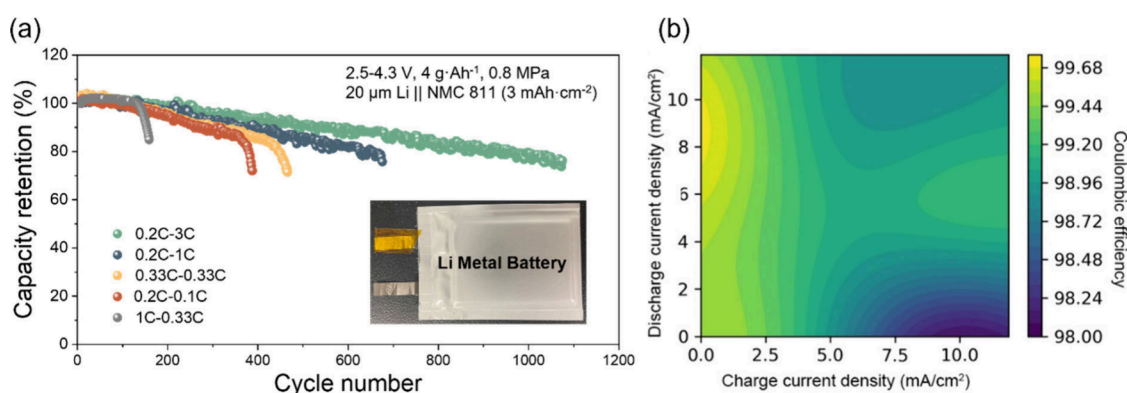
Figure 1. Cycling performance of SES Li metal cells under different charge/discharge rates: (a) capacity retention plots; (b) CE map based on the anode-free cell tests.

layer" inside the battery. This porous layer not only increases the cell thickness and impedance but also accelerates the electrolyte consumption, leading to even faster cell failure.[8,9] Another significant factor contributing to the failure of LMBs is the presence of inactive Li^0, which becomes trapped and isolated by the SEI layers due to electronic pathway loss during striping.[10] The presence of inactive Li^0 is observed via cryogenic electron microscopy (cryo-TEM), and the amount can be quantified by titration-gas chromatography (TGC).[11−13] The capacity loss due to inactive Li^0 depends on the electrolyte type and Li morphology. However, the combined impact of the SEI and inactive Li^0 has not yet been studied.

Tremendous amounts of research have proven that the interphase plays a critical role in improving the CE, and many approaches to interphase design have been developed. Advanced electrolytes with higher concentrations of salt or fluorinated molecules can form a more stable SEI that can passivate Li more effectively and reduce side reactions.[14−16] Anode surface treatments/coatings, which create artificial SEI and prevent contact between Li and liquid electrolyte, may improve the CE.[17,18] In other studies, researchers have developed architected anodes as hosts for Li, which enabled repeated plating/stripping with minimal Li loss.[19,20] However, many methods exhibited improvement only under certain conditions, such as slow charge rate or higher temperature, and often sacrifice energy density, resistance, and/or cost. These methods therefore cannot be applied to real-life applications and are far away from commercialization.[21,22] Moreover, it has long been noticed that asymmetric cycling protocols with faster discharge rates and slower charge rates benefit LMB cycling.[23] While the CE of LMBs is primarily determined by the SEI, the Li plating/stripping behavior also has unclear but non-negligible impacts. In addition to the intrinsic material challenges, practical applications pose conflicts with LMB advantages. For today's EVs, conventional Li-ion battery technology serves as the power source, which consists of multiple packs with cell modules arranged in parallel or series configurations based on voltage, current, or power requirements.[24] The goal for EVs is to achieve a driving range of over 300 miles on a single full battery charge. Consequently, to completely discharge the battery over this distance, it would require 5−10 h of driving time. In other words, the battery's average discharge rate equates to approximately a C/5 to C/10 rate, based on an average speed of 50 miles per hour. However, for LMBs, fast discharge rates (around 1C to 3C) are beneficial

but unrealistic for EV applications, where discharging time typically ranges from 20 min to 1 h.

To enhance the Li metal battery cycle life for EVs or similar applications, it is essential to develop a battery utilization strategy that ensures extended cycle life without compromising battery energy density. In this work, the cycling behavior of Li metal under different charge−discharge conditions is studied, and the degradation mechanisms are unveiled. The results indicate that reactions at the material level, including Li plating/stripping and SEI formation, are closely related to the charge/discharge rate. Under proper conditions, the CE can be improved, and the SEI residue can be reduced. This leads to a much longer cycling life with slower cell thickness growth, which also enables cell design optimization for high energy density. This study illustrates the mechanisms underlying improved performance achieved through slow charge/fast discharge, offering a potential approach to regulate fast discharge in EV applications and aiming to facilitate the development of commercial LMBs for EVs.

Figure 1a shows the cycling performance of the LMB with the capacity of 270 mAh and volumetric capacity of 960 Wh·L^{-1} at the staking level. The cell is fabricated by SES AI and filled with nonaqueous, high-concentration electrolytes. The results show that the cycling performance of LMBs is highly dependent on the charge/discharge rate (i.e., current density). With the same cathode loading (3 mAh·cm^{-2}) and sufficient electrolyte, the fast charge/slow discharge (1C−0.33C) cells only lasted 160 cycles. Here, 1C represents a current density of 3 mA·cm^{-2} and 0.33C is 1 mA·cm^{-2}. The slow charge, slow discharge condition (0.2C−0.1C), corresponding to 0.63−0.3 mA·cm^{-2} in current density, enabled 390 cycles, similar to the medium charge, medium discharge condition (0.33C−0.33C), which enabled 440 cycles. Interestingly, the slow charge and fast discharge conditions (0.2C−1C and 0.2C−3C) exhibited superior cycling performance up to 700 cycles and 1075 cycles, respectively. The differences in the cycling life are primarily attributed to the deterioration of the Li anode. As shown in the postanalysis of the cycled NMC cathodes (Figure S1), the test conditions (0.2C−1C and 0.33C−0.33C) had minimal impact on the cathode structure and performance after 300 cycles. The CE under different charge/discharge rates is systematically compared by using the NMC‖Cu anode-free cell format with the same cathode loading (Figure S2), in which no excess Li compensates for the capacity decay, and the CE can reflect the Li loss. Based on the tests, the color map of CE is derived, as shown in Figure 1b. It is apparent that the slow charge/fast
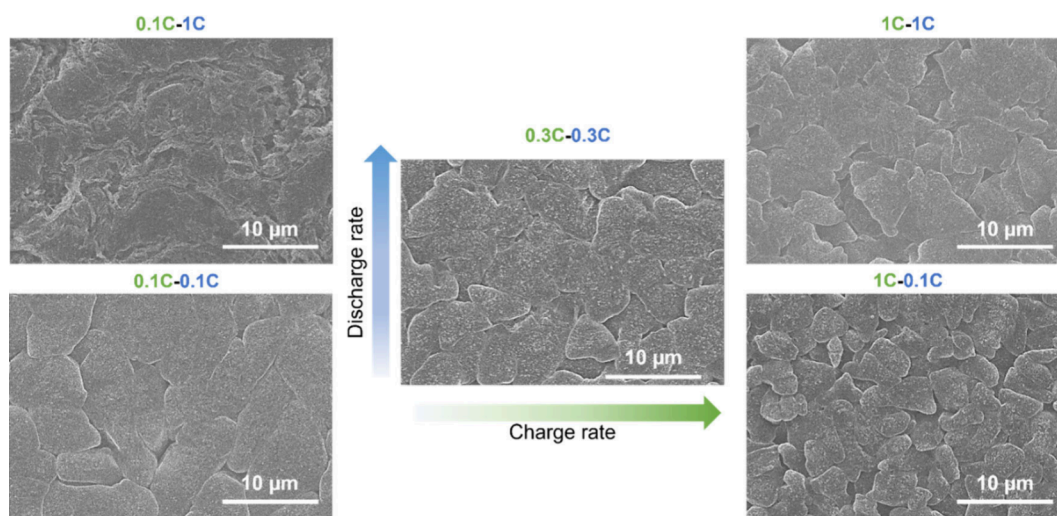
Figure 2. SEM top view images of Li anodes under different charge/discharge rates.

discharge region has the highest CE while the fast charge/slow discharge region has the lowest CE. Under 0.1C−3C charge/discharge, the CE can reach as high as 99.7%. On the contrary, under 3C−0.33C, the CE is only 98%. The charge−discharge rate fundamentally changed the cell behavior and improved the performance drastically.

To unveil the morphological differences of the Li anodes under different charge/discharge rates, cells were torn down after 50 cycles at 100% SOC. The cycled Li anodes of 0.33C−0.33C, 1C−0.1C, and 1C−1C electrodes all had a metallic, shining surface, as shown in Figure S3. In contrast, the central region of the 0.1C−0.1C electrode appeared darker than its periphery, while the 0.1C−1C electrode appeared black. These differences suggest that the charge/discharge rate influences the Li plating behavior. To further understand the different morphologies, the surface of the fully charged (100% SOC) electrodes was studied by using SEM. As depicted in Figure 2, the 0.1C−0.1C, 0.3C−0.3C, 1C−0.1C, and 1C−1C electrodes showed similar morphology: Li particles with different sizes were homogeneously dispersed on the surface. However, the 0.1C−1C anode presented a distinct feature, showing a film-like surface. Figure S4 illustrates the corresponding anode surface morphology after discharging to 0% SOC. Significant differences in morphology were observed for the 0.3C−0.3C, 1C−0.1C, and 1C−-1C electrodes compared to 100% SOC, where Li particles disappeared and the surface was covered by a film. Conversely, the morphology of the 0.1C−1C anode appeared nearly identical to its 100% SOC counterpart in Figure 2, indicating a minimal impact from discharge on surface morphology.

Cross-section morphologies of the cycled Li anodes under cycling conditions of 0.1C−1C, 0.33C−0.33C, and 1C−0.33C after 50 cycles at both 100% SOC and 0% SOC were examined to further reveal the Li deposition behavior, as shown in Figure 3. The 0.1C−1C electrode had a thin film on the Li surface, likely corresponding to the SEI. No distinct boundary was observed between the deposited Li and unused Li. After discharging to 0% SOC, the thickness of Li was reduced while the SEI layer remained on the surface. Cross-section images of both 100% SOC and 0% SOC indicated Li deposition beneath the SEI at this cycling rate, as shown in Figure 3a. In contrast, the Li metal anode cycled at 0.33C−0.33C exhibited a layer of SEI residue embedded between the deposited Li and unused
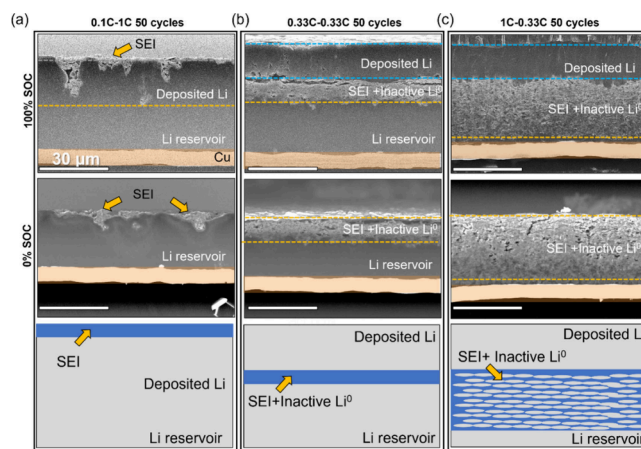
Figure 3. Cryo-SEM cross-section of Li anodes under different charge/discharge rates.

Li. This suggests that Li deposition occurs on top of the SEI, exposing fresh Li to the electrolyte and leading to additional SEI formation. Upon discharge, the deposited Li was stripped away, while the newly formed SEI accumulated on the surface of the anode, resulting in the buildup of a thick and porous SEI layer, as shown in Figure 3b. For the fast charge sample (1C−0.33C), at 100% SOC, a thick SEI layer appeared beneath the deposited Li, and the SEI was mixed with Li. After discharge, the deposited Li disappeared, leaving behind the thick SEI and Li layer. Li deposited above the SEI under this condition, like in 0.33C−0.33C, as shown in Figure 3c. The cross-sectional SEM images of Li anodes at 100% SOC after different cycles are shown in Figure S5. The upper row displays anodes cycled at 0.33C−0.33C, while the lower row shows anodes cycled at 0.1C−1C. The evolution of the morphology over the cycles clearly indicates that under 0.33C−0.33C conditions Li deposits above the SEI layer, leading to SEI accumulation and faster thickness growth. In contrast, under 0.1C−1C, Li from the cathode deposits beneath the SEI, resulting in minimal SEI accumulation on top of the deposited Li. The observed differences in appearance and morphology under slow charge/fast discharge conditions can be attributed to Li deposition beneath the SEI layer rather than above it. This suggests that the SEI formed under these conditions is fully
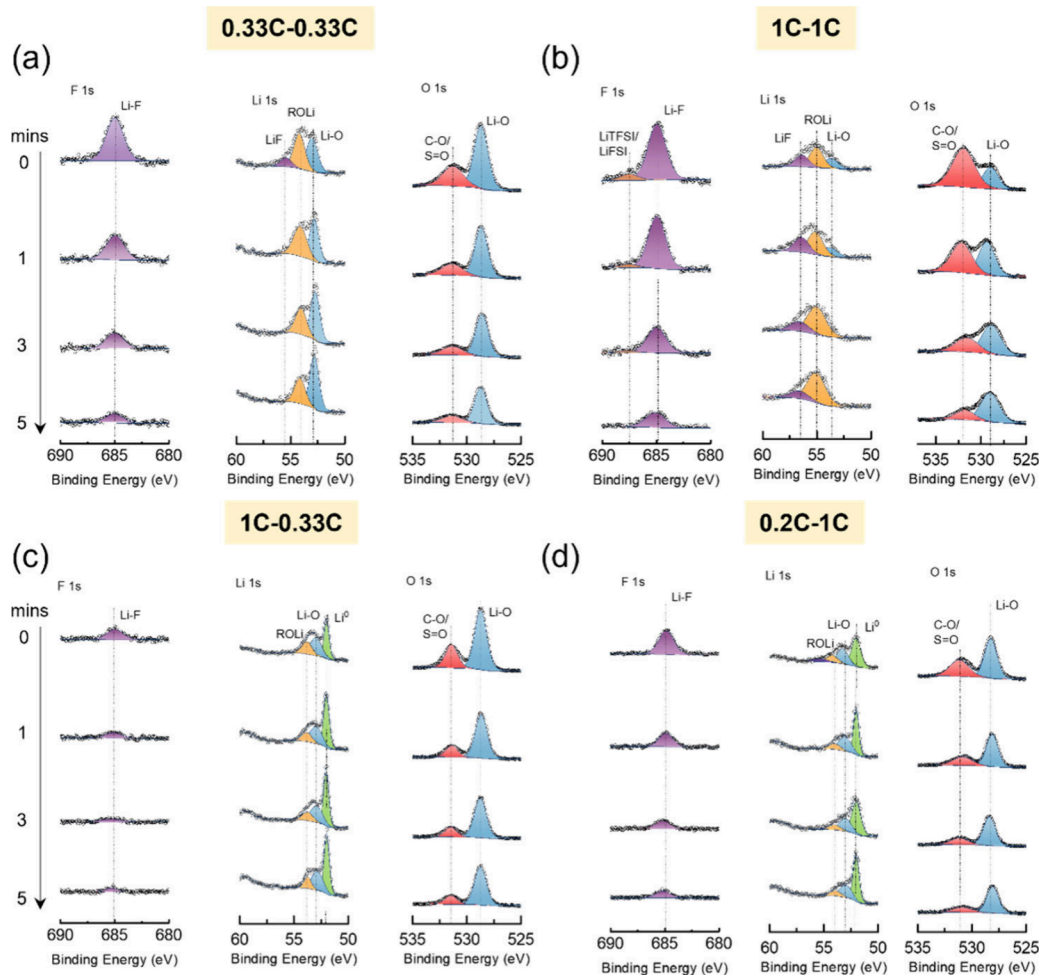
Figure 4. XPS spectra of Li anode after cycling at (a) 0.33C−0.33C; (b) 1C−1C; (c) 1C−0.33C, and (d) 0.2C−1C after 50 cycles.

passivating, effectively preventing side reactions between the Li metal anode and the electrolyte. As a result, this leads to higher CE and reduced SEI accumulation, which in turn extends the cycle life of the battery (Figure 1a). Another indirect evidence of the Li deposition changed under different cycling conditions is the interphase impedance difference. It is often considered that the first semicircle in the EIS plot can be ascribed to the SEI on the anode surface.[25] Our hypothesis is that if Li deposits beneath the SEI layer, the SEI thickness should remain similar between 0% and 100% SOC, resulting in a similar first semicircle in the EIS plot. Conversely, if Li deposits on top of the SEI layer, the SEI layer thickness would vary significantly, thicker at 0% SOC (due to multiple SEI layers) and thinner at 100% SOC (only one SEI layer), which would result in noticeable differences in the first semicircle. The experiment results support our hypothesis; as shown in Figure S6a, after 50 cycles under 0.1C−1C, the first semicircles of the 0% SOC and 100% SOC EIS plots are similar (around 0.02 Ω), indicating Li deposition beneath the SEI. However, after 50 cycles at 0.33C−0.33C, the first semicircle at 0% SOC (~0.07 Ω) is significantly larger than at 100% SOC (~0.017 Ω), suggesting Li deposition above the SEI (Figure S6b).

To explore the relationship between charge/discharge rates and Li deposition behavior, cells were tested under different conditions for 20 cycles and the morphology after cycling was examined, with the findings summarized in Figure S7. The x-axis represents the discharge rate, while the y-axis shows the

charge rate. The same map with the unit of current density is listed below. Based on the morphological characterizations, at 100% SOC, Li deposition can be divided into three scenarios: beneath the SEI (black blocks), above the SEI (white blocks), and a mixture of deposited Li and SEI (gray blocks). Specifically, Li tends to deposit beneath the SEI at a charge rate of 0.1C combined with a 0.3C discharge rate. Increasing the charge rate to 0.33C requires a discharge rate of 1.5C to ensure Li deposition beneath the SEI. When the discharge rate reaches 3C, Li can partially deposit under the SEI even at 1C fast charge rate. Furthermore, at a discharge rate of 10C, Li is likely to deposit beneath the SEI even at a higher charge rate of 3C. The results show that a more passivating SEI is formed under slow charge/fast discharge conditions, which conducts only Li ions. Conversely, an electronically conductive SEI layer forms under fast charge/slow discharge conditions, leading to Li deposition on top of the SEI. These findings highlight how the charge/discharge rates significantly affect the properties of the SEI layer.

The chemical components and structure of the SEI in cycled Li metal anodes were investigated via qualitative and quantitative approaches. Figure 4 and Figure S8 show the detailed SEI components in the cycled Li metal anode with different charge/discharge rates. The signals from the C 1s and the O 1s spectra are generally believed to reveal the solvent decomposition products. The F 1s, Li 1s, N 1s, and S 2p signals are usually used to analyze the salt decomposition
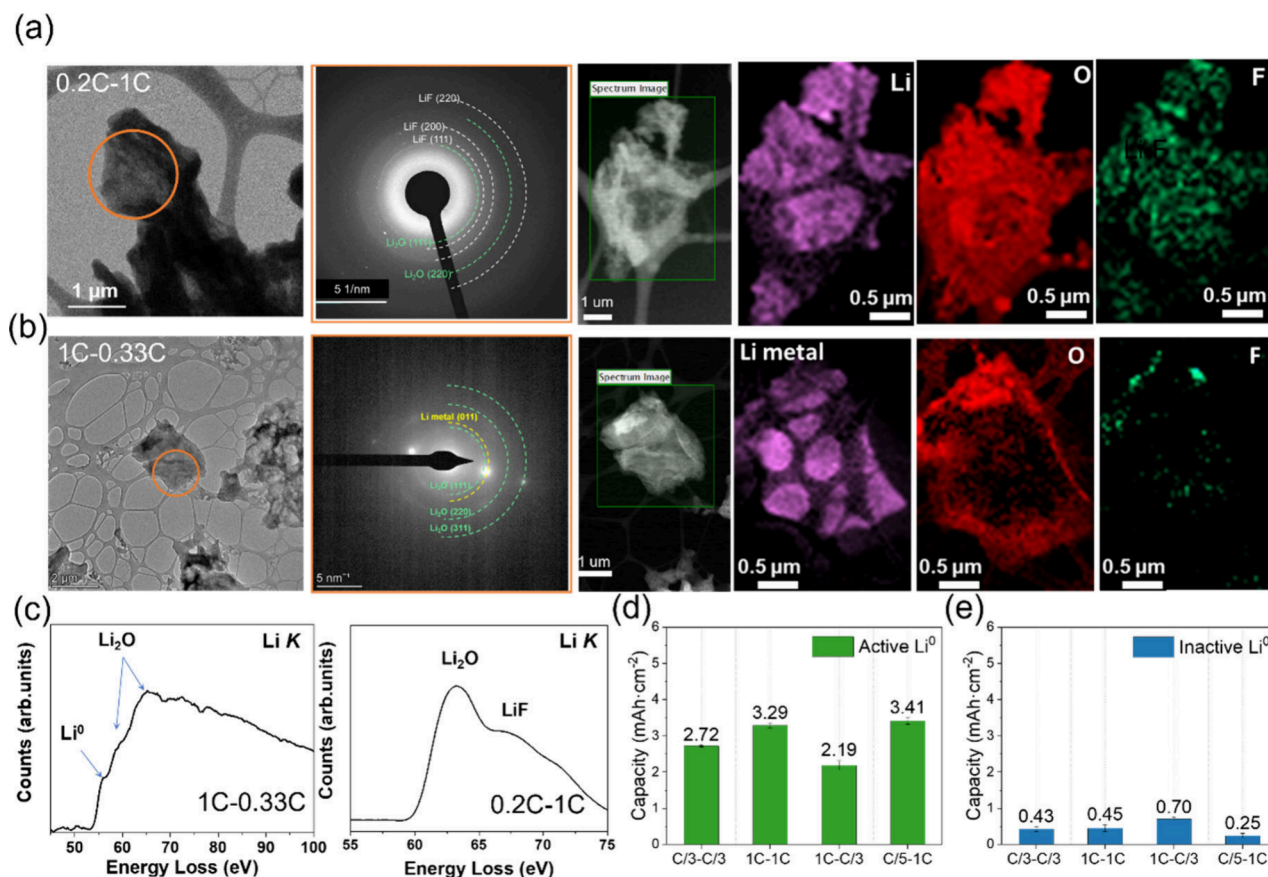
Figure 5. Low dose TEM image, SEAD pattern, and EELS mapping of Li anode after cycling at (a) 0.2C−1C; (b) 1C−0.33C after 50 cycles. (c) EELS spectra of Li K. (d) Active and (e) inactive Li^0 quantification results.

products. From the XPS spectra, the components of the SEI remained consistent across different cycling protocols comprising the same chemical substances, such as LiF, Li_2O, and various other organic and inorganic compounds. However, the ratio of each component within the SEI was significantly affected by the cycling conditions. When cycled at 0.33C−0.33C, the major inorganic components of the SEI were LiF and Li_2O. Additional signals in the N 1s and S 2p spectra in Figure S8a suggest the presence of Li salt residue and decomposition products. In contrast, cycling at 1C−1C showed a significant increase in the F 1s and S 2p peak intensities, as shown in Figure 4b and Figure S8b, indicating a higher rate of salt decomposition compared to the 0.33C−0.33C cycling conditions. Moreover, the disappearance of the Li_2O peak after etching suggests that Li_2O predominantly covers the SEI surface in the 1C−1C samples. Although an increase in C−O/S═O was observed in the O 1s spectra, similar C 1s results suggest that, compared to 0.33C−0.33C, salt decomposition is more prevalent than solvent decomposition when cycling at 1C−1C. A different trend was noted under the 1C−0.33C and 0.2C−1C cycling conditions, as shown in Figure 4c,d and Figure S8c,d. For 1C−0.33C, there was a decrease in the signal intensity for F 1s, N 1s, and S 2p but an increase in the intensity of the Li−O signal in the O 1s spectra Li−O signal, indicating that solvent decomposition dominates the SEI components compared to the 0.33C−0.33C condition. Additionally, Li^0 was detected in both 1C−0.33C and 0.2C−1C samples. However, in 1C−0.33C, it originates from the inactive Li^0, whereas in 0.2C−1C, it comes from active Li^0. This is evidenced by a more porous and thicker SEI

in the 1C−0.33C and a thinner SEI in the 0.2C−1C samples, as depicted in the surface morphology shown in Figure S9.

The structure of the SEI was further investigated via STEM/EELS, as shown in Figure 5 and Figures S10 and S11. When cycled at 0.33C−0.33C, the majority of the SEI components were amorphous. A small amount of crystalline LiF was detected, which is consistent with XPS results and suggests that Li−O is present in an amorphous structure. However, a large number of crystalline species were observed in the sample cycled at 0.2C−1C, with the major SEI components being crystalline LiF and Li_2O, as shown in Figure 5a. Additionally, in samples cycled at both 1C−1C and 1C−0.33C, inactive Li^0 was observed, surrounded by crystalline Li_2O. This is confirmed by the SEAD pattern and EELS spectra shown in Figure 5b,c and Figure S10b,c. This observation is further supported by the quantification results presented in Figure 5d. Active Li^0 was well-preserved in the sample cycled at 0.2C−1C, whereas it was mostly consumed in the sample cycled at 1C−0.33C. Along with an increase in inactive Li^0, a high amount of inactive Li^0 was detected in the sample cycled at 1C−0.33C.

The TEM and SEAD analyses of cycled Li metal anodes under various charge/discharge rates reveal notable differences in SEI composition and morphology. The 0.2C−1C sample exhibited the best performance with a compact and smooth SEI layer primarily composed of crystalline LiF and Li_2O, indicating that this structure provides the most stable protection. In contrast, the 1C−0.33C sample showed the poorest performance, characterized by a nonuniform SEI with prominent aggregations and moderate levels of Li_2O and LiF.
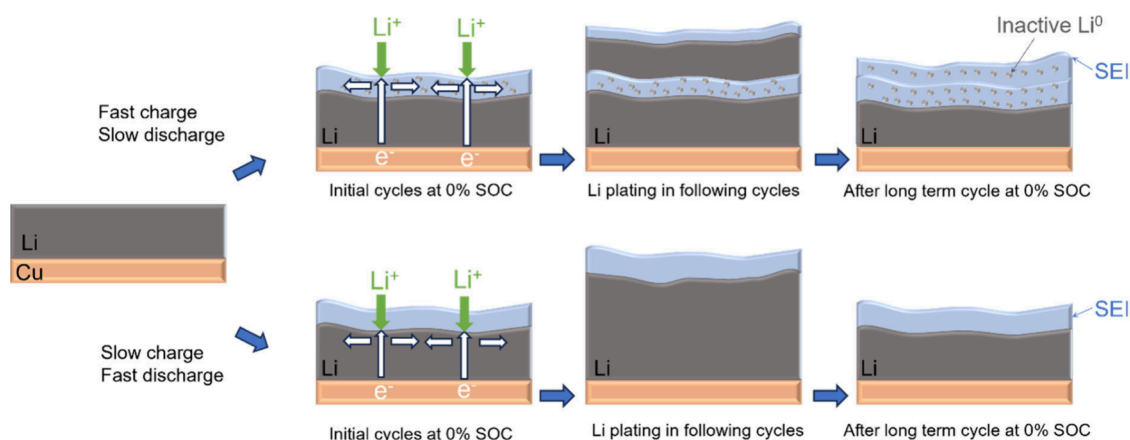
Figure 6. Diagram showing the Li deposition mechanisms under different cycling protocols.

The SEI in the 0.33C−0.33C sample was predominantly amorphous with trace amounts of LiF, while the 1C−1C sample displayed a porous SEI with mainly amorphous components and minor LiF content. These findings indicate that the crystallinity and uniformity of the SEI are crucial for enhancing performance, with the smooth, compact SEI in the 0.2C−1C sample being the most favorable for cycling stability. STEM and XPS results demonstrate that charge and discharge rates significantly affect the formation of SEI components, leading to variations in the SEI composition and properties. These changes in the component ratios play a pivotal role in determining battery performance and stability. Notably, the presence of inactive Li^0 raises safety concerns and may increase the electronic conductivity of the SEI layer, further impacting the battery's overall performance.

Slow charge facilitates Li nucleation and growth, which often results in a good Li morphology.[25] It is also possible that slow charge provides more time and less polarization, so that Li ions can transfer through the SEI and deposit underneath. However, the mechanism by which fast discharge facilitates Li deposition beneath the SEI needs further exploration. Notably, in cases of the symmetric charge/discharge and fast charge/slow discharge, Li deposited above the SEI layer, indicating that the Li nucleated on top of the SEI layer rather than directly on the Li foil underneath. Given that electronic conductivity is essential for nucleation, a plausible hypothesis is that under these conditions the SEI layer becomes electronically conductive. This is supported by XPS and TEM analyses presented in Figure 4 and Figure 5, suggesting that inactive Li^0 within the SEI may form an electronically conductive network. Such a network would facilitate electron transfer to the top of the SEI layer, thereby promoting Li nucleation at that location, as depicted in Figure 6. In contrast, under slow charge/fast discharge conditions, less inactive Li^0 is formed and the SEI layer maintains very low electronic conductivity, ensuring that Li nucleation can only occur on the Li foil surface underneath the SEI layer. Depositing Li beneath the formed SEI offers significant benefits, such as potentially reusing part of the SEI, leading to higher CE, longer cycling life, and slower dead Li thickness growth, as demonstrated in Figure 1 and Figure 3. Another indirect evidence of this hypothesis is the leakage current test, as shown in Figure S12, in which the slow charge/fast discharge sample showed a lower leakage current, indicating better passivation and less SEI formation. This phenomenon suggests that the Li deposition behavior is influenced by the ratio between the ionic conductivity (σ_i) and the electronic conductivity (σ_e) of the Li/electrolyte interphase. If the interphase has high σ_i/σ_e, Li ions are more likely to pass through the interphase and nucleate directly on the Li surface, resulting in deposition beneath the SEI. Conversely, if σ_i/σ_e is low, Li has a higher likelihood of nucleating on the electronically conductive interphase, leading to deposition above the SEI. This mechanism not only offers additional insights into existing studies but also provides valuable guidance for engineering the Li metal interface, including improvements to electrolytes, artificial SEIs, surface coatings, or 3D host structures. If an engineered interface fails to enable Li deposition underneath, then Li will instead deposit above it, causing SEI accumulation and eventual failure of the engineered interface. Therefore, when evaluating artificial SEIs or surface coatings, a critical consideration should be the location of Li deposition.

The next critical question is why less inactive Li^0 forms in the SEI layer under fast discharge conditions. A rational assumption is that the overpotentials required for Li plating and Li stripping are asymmetric. A higher driving force is required to strip the Li through the SEI layer completely. If the charge current density is the same or higher than the discharge current, Li tends to strip starting from the root area, leading to the tip losing electronic connection from the Li foil and leaving as inactive Li^0 in the SEI, making the SEI more electronically conductive. This process indicates that the discharge current needs to be sufficiently high to counterbalance the overpotentials associated with charging and discharging. Thus, the ratio between charge and discharge rates is crucial, not their absolute values. As illustrated in Figure S7, even with a 1C charge rate, a 3C discharge rate allows Li to deposit beneath the SEI. Another mechanism involves fast discharge, which creates a strong electric field in the electrolyte, inducing inactive Li^0 spatial progression toward the anode.[26,27] This electric field re-establishes electronic contact between the inactive Li^0 and the current collector, promoting the dissolution of the inactive Li^0. The higher the current density, the more pronounced this effect. A combination of these two mechanisms likely operates in real-world scenarios.

Based on the above findings, LMBs can effectively achieve a long cycling life by combining slow charging and fast discharging. However, this approach contrasts with common EV battery use, which often prefers fast charge/slow discharge. While charging rates can be controlled, discharge rates depend
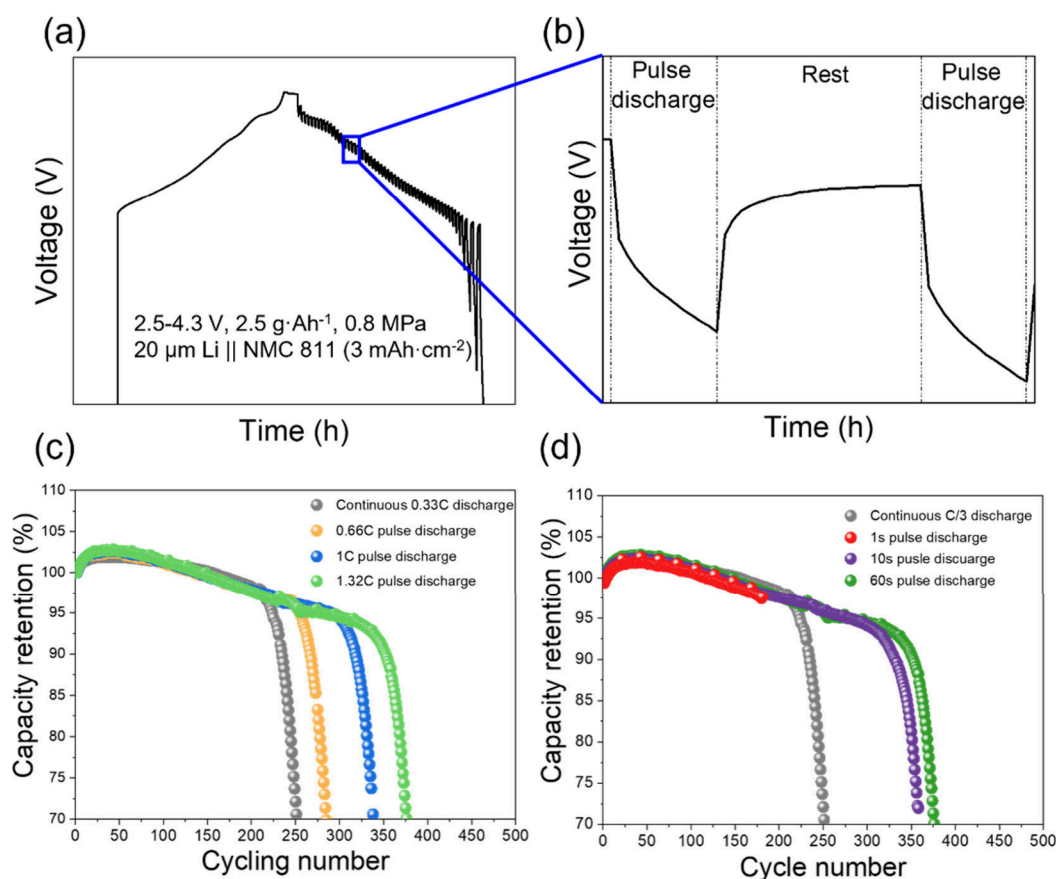
Figure 7. Pulse discharge protocol and cycling performance of 20 μm Li‖NMC 811 (3 mAh·cm^{-2}) pouch cell (2.5−4.3 V) with electrolyte amount of 2.5 g·Ah^{-1} and 0.8 MPa external pressure: (a, b) voltage curve of pulse discharge, (c) capacity retention with different pulse discharge currents, and (d) capacity retention with different pulse discharge time.

highly on customer demand. To accommodate fast discharging in practical scenarios, pulse discharging offers a promising solution. The design principle of this approach is based on the configuration of battery packs in a vehicle, where each pack contains multiple modules and each module comprises several cells. These battery packs/modules can be controlled individually by a battery management system (BMS). To achieve a longer discharge time, instead of simultaneously discharging all the packs/modules at a lower rate, it is feasible to selectively discharge each module at a higher rate and cycle through them sequentially, as illustrated in Figure S13. For instance, in a system with four battery modules in a pack, each module can be discharged at 1C for a designated time before switching to the next module. This method allows the entire battery system to operate at an overall discharge rate of 0.25C while each individual module discharges at 1C.

Figure 7a shows a working protocol for the intermittent fast pulse discharge, where during the discharge section the cell is discharged at a high rate for a short period followed by a rest period. The pulse current, pulse duration, and rest time are tailored to achieve the desired overall discharge rate. An optimized intermittent pulse discharging protocol can significantly extend the cycling life of LMBs. As shown in Figure 7b, the cells with lean electrolyte (2.5 g·Ah^{-1}) were charged at 0.33C and discharged at a rate equivalent to 0.33C but varied in pulse discharge current and rest time. The results indicate that the higher pulse discharge current correlates with a longer cycling life, aligning with previous fundamental studies. In Figure 7c, the cells were discharged at a rate

equivalent to 0.33C with the same pulse discharge current of 1.32C but varying lengths of pulse discharge time and rest periods. The findings suggest that the duration of pulse discharge should not be too short; longer discharge pulses appear to be necessary for optimal performance. With this cell design, the cycling performance of cells with 1.32C discharge pulse for 60 s followed by a rest period of 180 s exhibited a cycle life improvement of over 120 cycles compared to the 0.33C−0.33C benchmark, corresponding to a 48% enhancement in cycle life.

Full cell tests have revealed significant impacts of charge/discharge rates on the cycling life and CE of LMBs. With slow charge/fast discharge, the cells can reach over 1000 cycles, which is nearly 9 times higher than the cycling life under fast charge/slow discharge conditions. Cell teardown and postcycling analysis highlighted distinct Li deposition behaviors under different conditions. Slow charge/fast discharge enables Li to deposit beneath the formed SEI, making the SEI reusable and thus reducing the number of side reactions. TEM, XPS, and TGC discovered that the inactive Li^0 amount in the SEI varies depending on charge/discharge conditions. Fast charge/slow discharge resulted in the highest amount of inactive Li^0 in the SEI, while slow charge/fast discharge showed a negligible amount of inactive Li^0. Since Li nucleation requires electronic conductivity, it is plausible that the presence of inactive Li^0 in the SEI contributes to its electronic conductivity. Therefore, under fast charge and symmetric charge−discharge conditions, Li can nucleate and grow above the SEI layer. In contrast, with an electronically nonconductive SEI, as seen under slow

charge/fast discharge conditions, Li can penetrate only the SEI to nucleate on the underlying Li foil. To adapt our findings to real-world electric vehicle applications, we developed an intermittent pulse discharge protocol, analyzing the pulse current, duration, and rest periods. This optimized approach resulted in a 48% improvement in the cycle life, providing valuable insights for strategies aimed at extending the cycling life of LMBs.

■ ASSOCIATED CONTENT

Data Availability Statement

The data that support the findings of this study are available from the corresponding author upon reasonable request.

Ⓢ Supporting Information

The Supporting Information is available free of charge at https://pubs.acs.org/doi/10.1021/acsenergylett.4c03215.

> Experimental section, XRD, dQ/dV plot of cycled cathode; optical image, SEM surface and cross-section morphology of cycled Li metal anode; fitting of EIS data and XPS spectra; TEM and SEAD pattern of cycled Li metal and battery cycling data (PDF)

■ AUTHOR INFORMATION

Corresponding Authors

Ying Shirley Meng — *Pritzker School of Molecular Engineering, University of Chicago, Chicago, Illinois 60637, United States; Department of NanoEngineering, University of California San Diego, La Jolla, California 92093, United States;* ⓘ orcid.org/0000-0001-8936-8845; Email: shirleymeng@uchicago.edu

Hong Gan — *SES AI, Woburn, Massachusetts 01801, United States;* Email: hong@ses.ai

Authors

Yunya Zhang — *SES AI, Woburn, Massachusetts 01801, United States*

Wurigumula Bao — *Pritzker School of Molecular Engineering, University of Chicago, Chicago, Illinois 60637, United States;* ⓘ orcid.org/0000-0001-8109-1546

Ethan Jeffs — *SES AI, Woburn, Massachusetts 01801, United States*

Bin Liu — *SES AI, Woburn, Massachusetts 01801, United States*

Bing Han — *Pritzker School of Molecular Engineering, University of Chicago, Chicago, Illinois 60637, United States*

Weijie Mai — *SES AI, Woburn, Massachusetts 01801, United States*

Xinyu Li — *SES AI, Woburn, Massachusetts 01801, United States*

Weikang Li — *Department of NanoEngineering, University of California San Diego, La Jolla, California 92093, United States*

Yun Xu — *SES AI, Woburn, Massachusetts 01801, United States*

Bhargav Bhamwala — *Department of NanoEngineering, University of California San Diego, La Jolla, California 92093, United States*

Alex Liu — *Department of NanoEngineering, University of California San Diego, La Jolla, California 92093, United States*

Louis Ah — *Department of NanoEngineering, University of California San Diego, La Jolla, California 92093, United States*

Kun Ryu — *Pritzker School of Molecular Engineering, University of Chicago, Chicago, Illinois 60637, United States*

Complete contact information is available at:
https://pubs.acs.org/10.1021/acsenergylett.4c03215

Author Contributions

[#]Y.Z. and W.B. contributed equally. Y.Z., W.B., H.G., and Y.S.M. conceived the ideas. Y.Z and W.B. wrote the manuscript. E.J. and Y.Z. prepared electrodes and cycled the cells. E.J. and Y.Z. did cell teardown and SEM characterization. W.B., B.B., and L.A. performed TGC measurements. W.B. and A.L. performed cryo-FIB/SEM. B.H. performed TEM experiments and data analysis. W.B. and W.L. designed and conducted XPS experiments. All authors discussed the results and commented on the manuscript.

Notes

The authors declare the following competing financial interest(s): Ying Shirley Meng is a technical advisor for SES AI.

■ REFERENCES

(1) Whittingham, M. S.; Xiao, J. Fifty years of lithium-ion batteries and what is next? *MRS Bull.* **2023**, *48*, 1118−1124.

(2) Ma, J.; Li, Y.; Grundish, N. S; Goodenough, J. B; Chen, Y.; Guo, L.; Peng, Z.; Qi, X.; Yang, F.; Qie, L.; Wang, C.-A.; Huang, B.; Huang, Z.; Chen, L.; Su, D.; Wang, G.; Peng, X.; Chen, Z.; Yang, J.; He, S.; Zhang, X.; Yu, H.; Fu, C.; Jiang, M.; Deng, W.; Sun, C.-F.; Pan, Q.; Tang, Y.; Li, X.; Ji, X.; Wan, F.; Niu, Z.; Lian, F.; Wang, C.; Wallace, G. G; Fan, M.; Meng, Q.; Xin, S.; Guo, Y.-G.; Wan, L.-J. The 2021 battery technology roadmap. *J. Phys. D: Appl. Phys.* **2021**, *54*, No. 183001.

(3) Chen, S.; Dai, F.; Cai, M. Opportunities and challenges of high-energy lithium metal batteries for electric vehicle applications. *ACS Energy Lett.* **2020**, *5*, 3140−3151.

(4) Liu, J.; Bao, Z.; Cui, Y.; Dufek, E. J.; Goodenough, J. B.; Khalifah, P.; Li, Q.; Liaw, B. Y.; Liu, P.; Manthiram, A.; Meng, Y. S.; Subramanian, V. R.; Toney, M. F.; Viswanathan, V. V.; Whittingham, M. S.; Xiao, J.; Xu, W.; Yang, J.; Yang, X.-Q.; Zhang, J.-G. Pathways for practical high-energy long-cycling lithium metal batteries. *Nat. Energy* **2019**, *4*, 180−186.

(5) Wang, Q.; Liu, B.; Shen, Y.; Wu, J.; Zhao, Z.; Zhong, C.; Hu, W. Confronting the Challenges in Lithium Anodes for Lithium Metal Batteries. *Adv. Sci.* **2021**, *8*, No. 2101111.

(6) Wu, H.; Jia, H.; Wang, C.; Zhang, J.-G.; Xu, W. Recent Progress in Understanding Solid Electrolyte Interphase on Lithium Metal Anodes. *Adv. Energy Mater.* **2021**, *11*, No. 2003092.

(7) Hobold, G. M.; Lopez, J.; Guo, R.; Minafra, N.; Banerjee, A.; Meng, Y. S.; Shao-Horn, Y.; Gallant, B. M. Moving beyond 99.9% Coulombic efficiency for lithium anodes in liquid electrolytes. *Nat. Energy* **2021**, *6*, 951−960.

(8) Wang, H.; Huang, W.; Yu, Z.; Huang, W.; Xu, R.; Zhang, Z.; Bao, Z.; Cui, Y. Efficient lithium metal cycling over a wide range of pressures from an anion-derived solid-electrolyte interphase framework. *ACS Energy Lett.* **2021**, *6*, 816−825.

(9) Zhang, Y.; Heim, F. M.; Song, N.; Bartlett, J. L.; Li, X. New insights into mossy Li induced anode degradation and its formation mechanism in Li−S batteries. *ACS Energy Lett.* **2017**, *2*, 2696−2705.

(10) Lu, D.; Shao, Y.; Lozano, T.; Bennett, W. D.; Graff, G. L.; Polzin, B.; Zhang, J.; Engelhard, M. H.; Saenz, N. T.; Henderson, W. A.; Bhattacharya, P.; Liu, J.; Xiao, J. Failure Mechanism for Fast-Charged Lithium Metal Batteries with Liquid Electrolytes. *Adv. Energy Mater.* **2015**, *5*, No. 1400993.

(11) Fang, C.; Li, J.; Zhang, M.; Zhang, Y.; Yang, F.; Lee, J. Z.; Lee, M.-H.; Alvarado, J.; Schroeder, M. A.; Yang, Y.; Lu, B.; Williams, N.; Ceja, M.; Yang, L.; Cai, M.; Gu, J.; Xu, K.; Wang, X.; Meng, Y. S. Quantifying inactive lithium in lithium metal batteries. *Nature* **2019**, *572*, 511−515.

(12) Bao, W.; Fang, C.; Cheng, D.; Zhang, Y.; Lu, B.; Tan, D. H.S.; Shimizu, R.; Sreenarayanan, B.; Bai, S.; Li, W.; Zhang, M.; Meng, Y. S. Quantifying lithium loss in amorphous silicon thin-film anodes via titration-gas chromatography. *Cell Rep. Phya. Sci.* **2021**, *2*, No. 100597.

(13) Deng, W.; Yin, X.; Bao, W.; Zhou, X.; Hu, Z.; He, B.; Qiu, B.; Meng, Y. S.; Liu, Z. Quantification of reversible and irreversible lithium in practical lithium-metal batteries. *Nat. Energy* **2022**, *7*, 1031−1041.

(14) Ren, X.; Chen, S.; Lee, H.; Mei, D.; Engelhard, M. H.; Burton, S. D.; Zhao, W.; Zheng, J.; Li, Q.; Ding, M. S.; Schroeder, M.; Alvarado, J.; Xu, K.; Meng, Y. S.; Liu, J.; Zhang, J.-G.; Xu, W. Localized high-concentration sulfone electrolytes for high-efficiency lithium-metal batteries. *Chem* **2018**, *4*, 1877−1892.

(15) Yu, Z.; Rudnicki, P. E.; Zhang, Z.; Huang, Z.; Celik, H.; Oyakhire, S. T.; Chen, Y.; Kong, X.; Kim, S. C.; Xiao, X.; Wang, H.; Zheng, Y.; Kamat, G. A.; Kim, M. S.; Bent, S. F.; Qin, J.; Cui, Y.; Bao, Z. Rational solvent molecule tuning for high-performance lithium metal battery electrolytes. *Nat. Energy* **2022**, *7*, 94−106.

(16) Meng, Y. S.; Srinivasan, V.; Xu, K. Designing better electrolytes. *Science* **2022**, *378*, No. eabq3750.

(17) Zhou, H.; Yu, S.; Liu, H.; Liu, P. Protective coatings for lithium metal anodes: Recent progress and future perspectives. *J. Power Sources* **2020**, *450*, No. 227632.

(18) Huang, Z.; Lai, J.-C.; Liao, S.-L.; Yu, Z.; Chen, Y.; Yu, W.; Gong, H.; Gao, X.; Yang, Y.; Qin, J.; Cui, Y.; Bao, Z. A salt-philic, solvent-phobic interfacial coating design for lithium metal electrodes. *Nat. Energy* **2023**, *8*, 577−585.

(19) Cheng, Y.; Chen, J.; Chen, Y.; Ke, X.; Li, J.; Yang, Y.; Shi, Z. Lithium Host: Advanced architecture components for lithium metal anode. *Energy Storage Mater.* **2021**, *38*, 276−298.

(20) Chen, H.; Pei, A.; Wan, J.; Lin, D.; Vila, R.; Wang, H.; Mackanic, D.; Steinruck, H.-G.; Huang, W.; Li, Y.; Yang, A.; Xie, J.; Wu, Y.; Wang, H.; Cui, Y. Tortuosity effects in lithium-metal host anodes. *Joule* **2020**, *4*, 938−952.

(21) Albertus, P.; Babinec, S.; Litzelman, S.; Newman, A. Status and challenges in enabling the lithium metal electrode for high-energy and low-cost rechargeable batteries. *Nat. Energy* **2018**, *3*, 16−21.

(22) Xiao, J.; Shi, F.; Glossmann, T.; Burnett, C.; Liu, Z. From laboratory innovations to materials manufacturing for lithium-based batteries. *Nat. Energy* **2023**, *8*, 329−339.

(23) Niu, C.; Lee, H.; Chen, S.; Li, Q.; Du, J.; Xu, W.; Zhang, J.-G.; Whittingham, M. S.; Xiao, J.; Liu, J. High-energy lithium metal pouch cells with limited anode swelling and long stable cycles. *Nat. Energy* **2019**, *4*, 551−559.

(24) Arora, S.; Shen, W.; Kapoor, A. Review of mechanical design and strategic placement technique of a robust battery pack for electric vehicles. *Renewable Sustainable Energy Rev.* **2016**, *60*, 1319−1331.

(25) Choi, W.; Shin, H.-C.; Kim, J. M.; Choi, J.-Y.; Yoon, W.-S. Modeling and applications of electrochemical impedance spectroscopy (EIS) for lithium-ion batteries. *J. Electrochem. Sci. Technol.* **2020**, *11*, 1−13.

(26) Liu, Y.; Xu, X.; Sadd, M.; Kapitanova, O. O.; Krivchenko, V. A.; Ban, J.; Wang, J.; Jiao, X.; Song, Z.; Song, J.; Xiong, S.; Matic, A. Insight into the Critical Role of Exchange Current Density on Electrodeposition Behavior of Lithium Metal, Advanced. *Science* **2021**, *8*, No. 2003301.

(27) Liu, F.; Xu, R.; Wu, Y.; Boyle, D. T.; Yang, A.; Xu, J.; Zhu, Y.; Ye, Y.; Yu, Z.; Zhang, Z.; Xiao, X.; Huang, W.; Wang, H.; Chen, H.; Cui, Y. Dynamic spatial progression of isolated lithium during battery operations. *Nature* **2021**, *600*, 659−663.